Supplementary Information

Self-induced "electroclick" immobilization of a copper complex onto self-assembled monolayers on a gold electrode

Antoine Gomila,[a] Nicolas Le Poul,[a] Nathalie Cosquer,[a] Jean-Michel Kerbaol,[a] Jean-Marc Noël,[a] Madhusudana T. Reddy,[a] Ivan Jabin,[b] Olivia Reinaud,[c] Francoise Conan*[a] and Yves Le Mest*[a]

[a]*Laboratoire de Chimie, Electrochimie Moléculaires et Chimie Analytique, UMR 6521 CNRS, Université de Brest, 29238 Brest, France ;* [b]*Laboratoire de Chimie Organique, Université Libre de Bruxelles (U.L.B.), Brussels, Belgium and* [c]*Laboratoire de Chimie et Biochimie Pharmacologiques et Toxicologiques, UMR 8601 CNRS, Université Paris Descartes, 75006 Paris, France*

Experimental Section.

Chemicals. Organic solvents were distilled on CaH_2 except THF and diethyl ether on Na/benzophenone. Anhydrous "extra-dry" dichloromethane (H_2O < 30 ppm, Acros), DMF (99.8%, Aldrich) and acetonitrile (99.9% BDH, VWR) were used as received and kept under N_2 in the glovebox. All solvents were thoroughly degassed before use. NBu_4PF_6 was synthesized from NBu_4OH (Fluka) and HPF_6 (Aldrich). It was then purified, dried under vacuum for 48 hours at 100° C, then kept under N_2 in the glovebox. The starting material (6-bromo-2-pyridyl)methyl)bis(2-pyridylmethyl)amine (6-BrTMPA) **1** was prepared according to literature.[1] The synthesis of 11-azidoundecane-1-thiol was performed following a previously described procedure.[2] All other chemicals were of reagent grade and were used without purification.

General experimental methods. Elemental analyzes were performed by the "Service Central d'Analyses du CNRS", Gif-sur-Yvette, France. NMR spectra were recorded on a Bruker DRX 500 MHz apparatus. IR spectra were recorded on a Nicolet Nexus FT-IR instrument (KBr pellets). EPR spectra were run on a Bruker Elexys spectrometer (X-band). Vis-NIR spectroscopy was performed with a JASCO V-670 spectrophotometer. The electrochemical studies in organic solvents were performed in a glovebox (Jacomex) (O_2 < 1 ppm, H_2O < 1 ppm) with a home-designed 3-electrodes cell (WE: Pt, RE: Pt, CE: Ag). The potential of the cell was controlled by an AUTOLAB PGSTAT 302 (Ecochemie) potentiostat monitored by a computer. Ferrocene was added at the end of each experiment to determine redox potential values. Voltammetry in aqueous electrolyte was performed in reference to a calomel reference electrode. The redox potential of ferrocene was determined *vs.* SCE (0.40 V) in $MeCN/NBu_4PF_6$.

Preparation of gold electrodes for SAMs grafting. A commercial gold removable tip electrode (Metrohm) was used. Before modification, the surface of the gold electrode (A = 0.07 cm^2) was prepared by a classical procedure by polishing on a slurry with alumina (3 µm). It was then sonicated in water (Millipore, 18 MΩ) and cycled between +0.5 and 1.4 V *vs.* SCE in H_2SO_4 0.1 mM (40 scans) to remove gold oxide, then washed with water, then ethanol and dried under slight flow of N_2 before being introduced in the solution containing thiol compounds. This procedure allowed the use of a same electrode with a resurrected appropriate Au surface condition.

[1] M. Merkel, D. Schnieders, S. M. Baldeau and B. Krebs, *Eur. J. Inorg. Chem.*, 2004, 783.
[2] J. P. Collman, N. K. Devaraj and C. E. D. Chidsey, *Langmuir,* 2004, **20**, 1051.

Synthesis of (6-trimethylsilylethynyl-2-pyridylmethyl)bus(2-pyridylmethyl)amine (Ligand 6-tmseTMPA) (Compound 2)

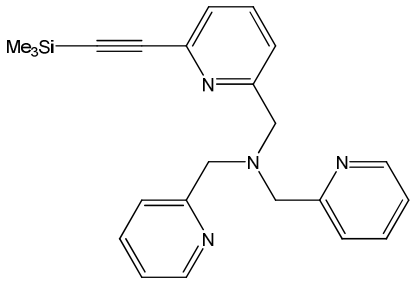

6-tmseTMPA

To a solution of [(6-bromo-2-pyridyl)methyl]bis(2-pyridinylmethyl)amine (6-BrTMPA) **1** (925 mg, 2.50 mmol) in 40 mL of a degassed 1:1 mixture of THF and diisopropylamine were added $[PdCl_2(PPh_3)_2]$ (106 mg, 0.15 mmol) and copper (I) iodide (48 mg, 0.25 mmol). Ethynyltrimethylsilane (0.71 mL, 5.00 mmol) was then added dropwise and the mixture was stirred for two days at room temperature. After cooling at 0°C, the precipitate was filtered off and then the solvent was removed under reduced pressure. The resulting residue was dissolved in 20 mL of dichloromethane washed three times with 50 mL of water and extracted twice with 100 mL of dichloromethane. The organic layers were combinated, dried on sodium sulfate and condensed to dryness. The crude red oil was dissolved into a minimum amount of dichloromethane. Chromatography on a column of neutral alumina with dichloromethane/methanol 99:1 as eluent afforded, after evaporation, (6-tmseTMPA) **2** as an orange powder which was not furthermore purified (620 mg; 1.60 mmol; yield: 64%).

^{1}H NMR (500 MHz, $CDCl_3$): δ (ppm) = 8.53 (d; J = 4.1 Hz; 2H; *CHN*); 7.65-7.52 (m; 6H; *CH*); 7.32 (t ; 1H; *CH*); 7.14 (t; 2H; *CH*); 3.89 (s; 2H; CH_2); 3.87 (s; 4H; CH_2); 0.26 (s; 9H; CH_3).^{13}C NMR(125.8 MHz, $CDCl_3$); **IR** (KBr pellet): ν(C≡C) = 2156 cm^{-1}.

Synthesis of (6-trimethylsilylethynyl-2-pyridylmethyl)bis(2-pyridylmethyl)amine (Ligand 6-TMPA) (Compound 3)

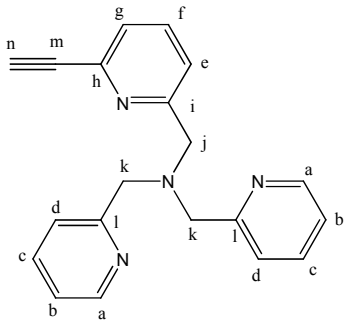

6-eTMPA

Potassium fluoride (560 mg, 7.64 mmol) was added to a solution of (6-trimethylsilylethynyl-2-pyridylmethyl)bis(2-pyridylmethyl)amine **2** (6-tmseTMPA) (620 mg; 1.60 mmol) in a 1:1 MeOH/THF mixture (20 mL). The reaction was stirred for two days at room temperature, and then solvents were removed under low pressure. The resulting brown residue was dissolved in CH_2Cl_2 (20 mL), filtered off to remove potassium fluoride in excess and then washed with water (2 x 50 mL). The aqueous layer was extracted with CH_2Cl_2 (2 x 100 mL) and the combined organic layers were filtered and then concentrated under reduced pressure. The crude product was purified by column chromatography on alumina (CH_2Cl_2/methanol, 99:1), yielding pure (6-trimethylsilylethynyl-2-pyridylmethyl)bis(2-pyridylmethyl)amine **3** (6-eTMPA) (385 mg, 95%) as a pale orange solid.

^{1}H NMR (500 MHz, $CDCl_3$) : δ(ppm) = 8.54 (d; *J* = 4.1 Hz; 2H; *CHN*) ; 7.69-7.63 (m; 4H; *CH*) ; 7.56 (d; *J* = 7.8 Hz; 2H, *CH*) ; 7.35 (t;1H; *CH*) ; 7.13 (t; 2H; *CH*) ; 3.91 (s; 2H; CH_2) ; 3.90 (s; 4H ; CH_2) ; 3.15 (s; 1H ; *CH*). **^{13}C NMR (125.8 MHz, $CDCl_3$)** δ(ppm) = 160.29 (Ci); 159.17(Cl); 149.13 (Ca); 141.38 (Ch); 136.60 (Cf); 136.41 (Cc); 125.77 (Cg); 123.00 (Cd); 122.74 (Ce);122.04 (Cb); 82.89 (Cn); 77.30(Cm); 60.18 (Ck); 60.01 (Cj) **IR** (KBr pellet): ν(≡C-H) = 3252; ν(**C≡C**H) = 2113 cm^{-1}; **Analysis** calculated for $C_{20}H_{18}N_4$ 0.05 CH_2Cl_2: C, 75.6; H, 5.7; N, 17.6. Found: C, 75.6; H, 5.7; N, 17.0.

Synthesis of [Cu(6-eTMPA)(H_2O)](CF_3SO_3)$_2$ (Compound 4)

Addition of trifluoromethanesulfonate Cu^{II} (121 mg, 0.33 mmol) to an acetone solution (10 mL) of ligand 6-eTMPA **3** (105 mg, 0.33 mmol) afforded a blue-green solution. After stirring (ca. 30 min), the solution was filtered off and reduced to dryness under low pressure. The resulting solid was then dissolved in THF (5 mL). Slow diffusion of pentane in this solution afforded blue-green single crystals suitable for X-ray analysis. Yield 190 mg (83 %). **IR** (KBr pellet): ν(C≡C-H);) = 3254 cm^{-1}; ν(**C≡C**H);) = 2113 cm^{-1} ; δ(C≡C-H) = 640 cm^{-1}. **Analysis** calculated for $C_{22}H_{20}CuF_6N_4O_7S_2$: C, 38.1; H, 2.9; N, 8.1. Found: C, 38.2; H, 2.9; N, 8.0.

XRD analysis of $Cu(6\text{-}eTMPA)(H_2O)](CF_3SO_3)_2$ (Compound 4)

Compound **4**, crystallizes in the monoclinic space group *P*21/*n* (Table S1). The asymmetric unit contains one copper atom, one organic ligand, one molecule of water and two trifluoromethanesulfonate anion located on general positions (see full ORTEP drawing on Fig. S1). The metal core in **4** lies in a pseudo-octahedral environment, as already observed for several Cu-TMPA derivatives.[3] N-Cu bonds length vary from 1.985 to 2.258 Å and the adjacent angles NCuN within the pseudo-octahedral core vary from 82.52 to 99.00° (Table S2). The sixth position is occupied by an oxygen atom of a triflate anion in *trans* to the 6-ethynylpyridine group. The Cu•••O(2) distance (2.704(2) Å) indicates a slight interaction between these atoms. The second triflate operates as a counter-ion. The arrangement of the atoms can be compared with those of $[Cu(TLA)(C_2O_4)]$ (TLA = tris(6-methyl-2-pyridyl)methylamine) in which Cu^{II} lies on the square-plane of two oxygen atoms of the oxalate anion, one amine and one pyridine nitrogen atom of the tetradentate ligand.[4] It is worthy to note that the copper-nitrogen distance arising from the substituted pyridyl group is longer than the others (2.258(2) Å), traducing certainly a *trans* electronic effect of the coordinated triflate anion on the Cu-N distance. The C(19)-C(20) distance of 1.175(2) Å, the H(20)-C(20)-C(19) and the C(18)-C(19)-C(20) angles respectively of 178.8(2)° and 177.3(2)°, corroborate the sp hybridization of those carbon atoms. At last, examination of the intermolecular distances clearly reveals hydrogen bonding which involves aqua ligands and triflate counter-ions (Table S3).

[3] *(a)* L. Zhu, O. dos Santos, C. W. Koo, M. Rybstein, L. Pape and J. W. Canary, *Inorg. Chem.*, 2003, **24** , 7912. *(b)* Z. He, J. Chaimungkalanont, D. C. Craig and S. B. Colbran, *J. Chem. Soc. Dalton Trans*., 2000,1419. *(c)* R. R. Jacobson, Z. Tyeklar, K. D. Karlin, and J. Zubieta, *Inorg. Chem.*, 1991, **30**, 2035.

[4] Z.-H. Zhang, H.-L. Yang, Y. Tang, Z.-H. Ma and Z.-A. Zhu, *Trans. Met. Chem*., 2004, **29**, 590.

Table S1. Crystal data and structure refinement for compound **4**.

Empirical formula	$C_{22}H_{20}CuF_6N_4O_7S_2$
M	694.08
Crystal system	Monoclinic
Space group	P 21/n
a / Å *b* / Å *c* / Å	9.4555(6) 27.9373(12) 11.2480(7)
β / °	112.820(7)
V / Å^3	2738.7(3)
Z	4
D_c / g cm^{-3}	1.683
μ. / mm^{-1}	1.041
F(000)	1404
T / K	170(2)
θ Range /°	2.75 -30.51
hkl Ranges	±13;-38-39; -15-14
Reflect. col. / unique, *R*(int)	27447 / 8254, 0.0335
Completeness to θ	30.51 98.7 %
Data / restr. / param.	8254 / 0 / 391
Goodness of fit on F^2	0.963
Fin. *R* [$I>2\sigma(I)$] *R*1; ω*R*2	0.0339; 0.0754
R ind. (all data) *R*1; ω*R*2	0.0681; 0.0837
Large. diff. peak and hole (e.A^{-3})	0.432 and -0.263

Table S2. Selected bond lengths (Å) and bond angles (°) for compound **4**

N(1)-Cu(1)	2.042 (2)	O(7)-Cu(1)-O(2)	84.80(6)
N(2)-Cu(1)	1.985 (2)	O(7)-Cu(1)-N(2)	99.00(6)
N(3)-Cu(1)	1.986 (2)	O(7)-Cu(1)-N(3)	92.43(6)
N(4)-Cu(1)	2.258 (2)	N(2)-Cu(1)-N(3)	164.02(6)
O(7)-Cu(1)	1.977 (2)	O(7)-Cu(1)-N(1)	165.85(7)
O(2)-Cu(1)	2.704(2)	N(2)-Cu(1)-N(1)	82.95(6)
C(19)-C(20)	1.175(3)	N(3)-Cu(1)-N(1)	83.29(6)
C(6)-N(2)-Cu(1)	127.2(2)	O(7)-Cu(1)-N(4)	110.51(6)
C(2)-N(2)-Cu(1)	113.4 (2)	N(2)-Cu(1)-N(4)	102.33(6)
C(8)-N(3)-Cu(1)	114.6(2)	N(3)-Cu(1)-N(4)	83.85(5)
C(12)-N(3)-Cu(1)	126.2(3)	N(1)-Cu(1)-N(4).	82.52(6)
C(18)-N(4)-Cu(1)	130.0(2)	H(20)-C(20)-C(19)	178.8(2)
C(14)-N(4)-Cu(1)	107.7(2)	C(18)-C(19)-C(20)	177.3(2)
		N(1)-Cu(1)-O(2)	81.23(2)

Specific comments on spectroscopic and electrochemical results

EPR and Vis-NIR studies

The axial signal obtained in EPR for **4** in MeCN (Fig. S2) features a Cu^{II} complex in a square-based geometry (SBP). The spectrum shows the existence of a second species, which has not been detected by room temperature voltammetry. EPR signature in DMF (Fig. S3) and CH_2Cl_2 (Fig. S4) are similar with a large peak at $g \approx 2.05$ and four equidistant peaks at weaker field associated to $g_{//}$ ($g_{//} \approx 2.25$, $A_{//} \approx 160$ G). This means that the complex **4** remains in the same geometry (SBP) in each medium, and that it is little affected by the nature of the fifth ligand (solvent molecule).

Vis-NIR spectroscopy in these solvents (Fig. S5, S6, S7) lead to the same conclusions, with the observation of a maximum absorption around 800 nm with a shoulder at *ca* 650 nm. Each spectrum (EPR and Vis-NIR) has been compared to this obtained in the same experimental conditions for the parent complex $[Cu^{II}(TMPA)(H_2O)]^{2+}$. This complex shows contrastly to compound **4**, a typical trigonal bipyramidal signature in the studied solvents.

Voltammetric studies

The voltammetry at a Pt working electrode of **4** DMF/NBu_4PF_6 (Fig. S9) shows a quasi-reversible system at $E_{1/2}$ = -0.55 V vs Fc (ΔE_p = 108 mV at 0.1V s^{-1}). By comparison with MeCN ($E_{1/2}$ = -0.33 V, ΔE_p = 64 mV), this result emphasized the influence of the fifth ligand on the redox potential of the system and on the reorganization of the complex through the electron transfer reaction (Fig. S8). As already observed for the $[Cu(TMPA)L]^{2+}$ compound, the shift in $E_{1/2}$ value results probably from the higher donor ability of DMF vs MeCN.[5] Also, higher peak separation (108 mV vs 64 mV), indicates that the Cu-6etmpa complex rearranges more drastically at Cu(I) in DMF, probably due to the low affinity between the metal ion and the O-donor. In CH_2Cl_2, the voltammetry is more complicated, since a broad oxidation peak is observed on the reverse scan (Fig. S10). This shows that a large reorganization operates after reduction, with eventually decoordination of the fifth ligand (H_2O) in this solvent. Interestingly and conversely to the copper-TMPA analog, the complex seems to unreact at the Cu(I) state with CH_2Cl_2: the anodic peak intensity does not disappear of at low scan rate and a new reversible system is not concomitantly observed at lower potential ($[Cu^{II/I}Cl(TMPA)]^{n+}$ complexes).

[5] N. Le Poul; B. Douziech, J. Zeitouny,; G. Thiabaud,; H. Colas, F. Conan, N. Cosquer, I. Jabin, C. Lagrost, P. Hapiot, O. Reinaud, and Y. Le Mest, *J. Am. Chem. Soc.*, 2009, **131**, 17800.

AC impedance studies

Impedance studies were performed on a Au bare and an 11-azido-undecane-1-thiol modified Au electrodes (A = 0.07 cm^2) in H_2O/KNO_3 containing equimolar amounts of $K_3Fe(CN)_6$ and $K_4Fe(CN)_6$ (Fig. S13). The analysis of the complex-plane plots (Z' *vs* $-Z''$) in reference to a classical equivalent circuit for an electrochemical cell[6] allows the determination of charge transfer resistance R_{ct} at the electrode/solution interface. The large difference in values of R_{ct} obtained between the bare and grafted electrodes (50 $\Omega.cm^2$ vs 21 $k\Omega.cm^2$) indicates that the electron transfer reaction is inhibited by the thiol. This supports voltammetric results in the same solution, with the loss of redox response for the thiol-modified working Au electrode (Fig. S12). Also, the same measurements (voltammetry and impedance) performed with another redox probe ($[Ru(NH_3)_6]Cl_3$ showed the same slowing down effect of the azido-alkane-thiol monolayer on the kinetics of electron transfer (Fig. S14 and S15).

[6] (a) R. P.Janek, W. R.Fawcett and A.Ulman, *Langmuir* 1998, **14**, 3011. (b) E.Sabatini, J.Cohen-Bouliaka, M. Bruening and I.Rubinstein, *Langmuir* 1993, **9**, 2974.

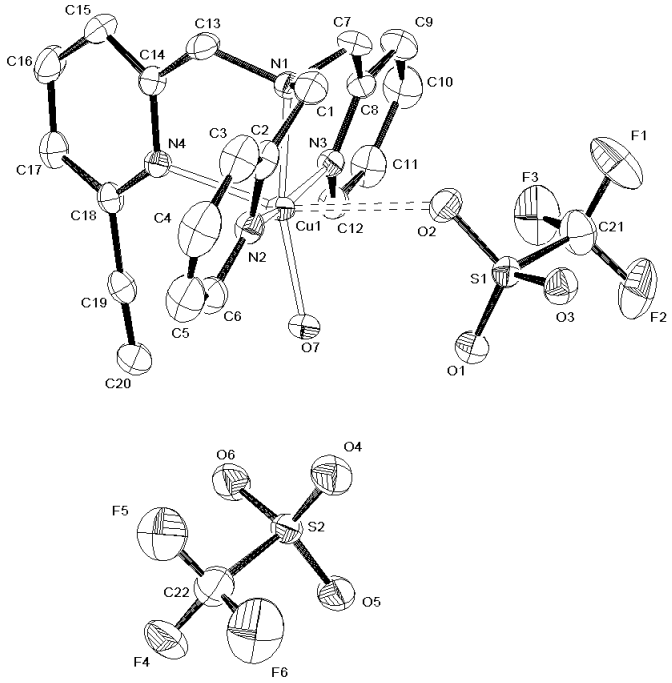

Fig. S1 ORTEP representation of the structure and atomic labeling scheme for the complex $[Cu(6\text{-eTMPA})(H_2O)](CF_3SO_3)_2$ (**4**). Hydrogen atoms are omitted for clarity.

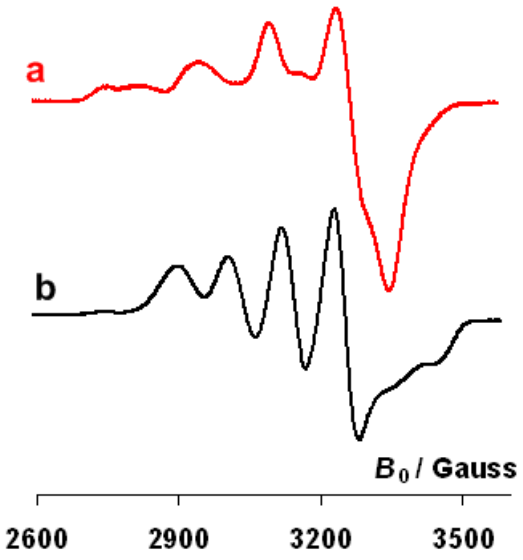

Fig. S2 EPR spectra of a) $[Cu(6\text{-eTMPA})(H_2O)](CF_3SO_3)_2$ (**4**) and b) $[Cu(TMPA)(H_2O)](CF_3SO_3)_2$ in $MeCN/NBu_4PF_6$ at T = 150 K.

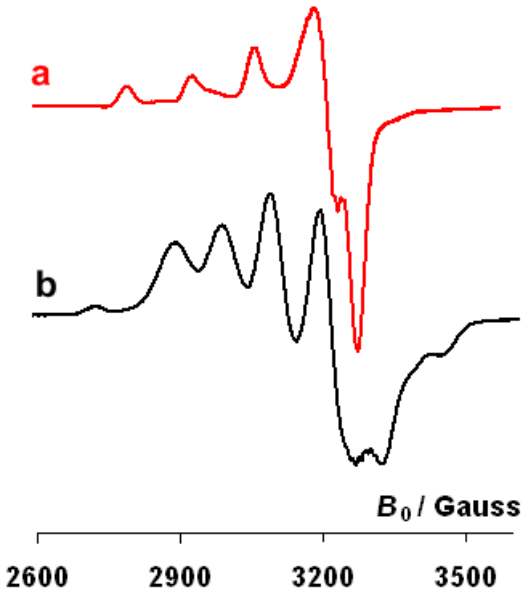

Fig. S3 EPR spectra of a) $[Cu(6\text{-eTMPA})(H_2O)](CF_3SO_3)_2$ (**4**) and b) $[Cu(TMPA)(H_2O)](CF_3SO_3)_2$ in DMF/NBu_4PF_6 at T = 150 K.

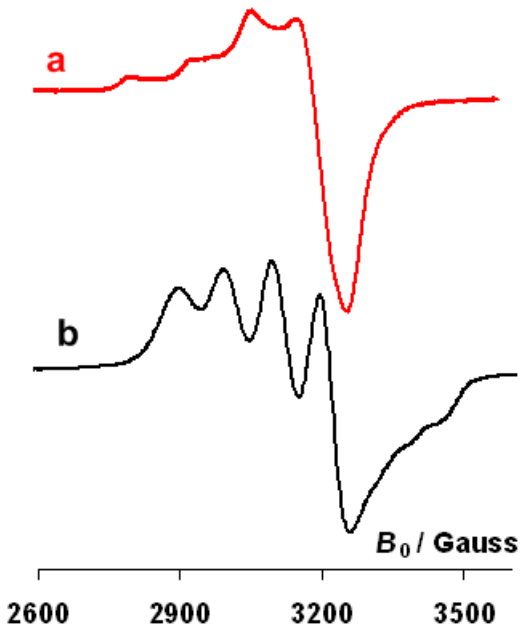

Fig. S4 EPR spectra of a) $[Cu(6\text{-eTMPA})(H_2O)](CF_3SO_3)_2$ (**4**) and b) $[Cu(TMPA)(H_2O)](CF_3SO_3)_2$ in CH_2Cl_2/NBu_4PF_6 at T = 150 K.

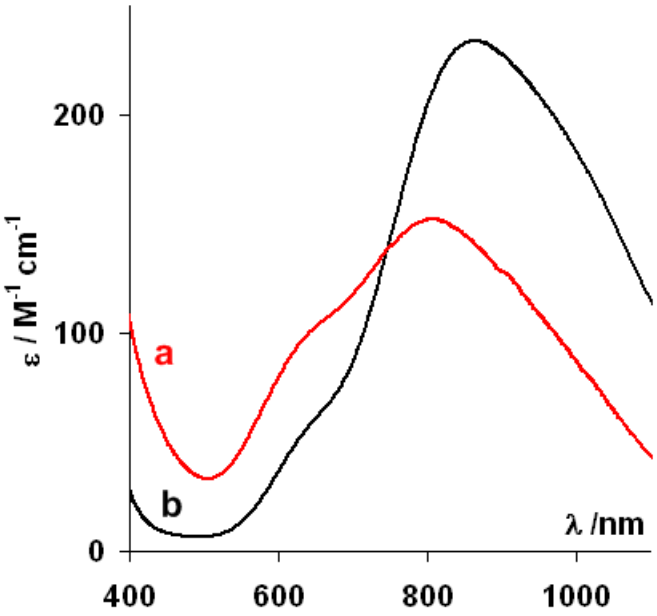

Fig. S5 UV-Vis spectra of a) $[Cu(6\text{-}eTMPA)(H_2O)](CF_3SO_3)_2$ (**4**) and b) $[Cu(TMPA)(H_2O)](CF_3SO_3)_2$ in MeCN.

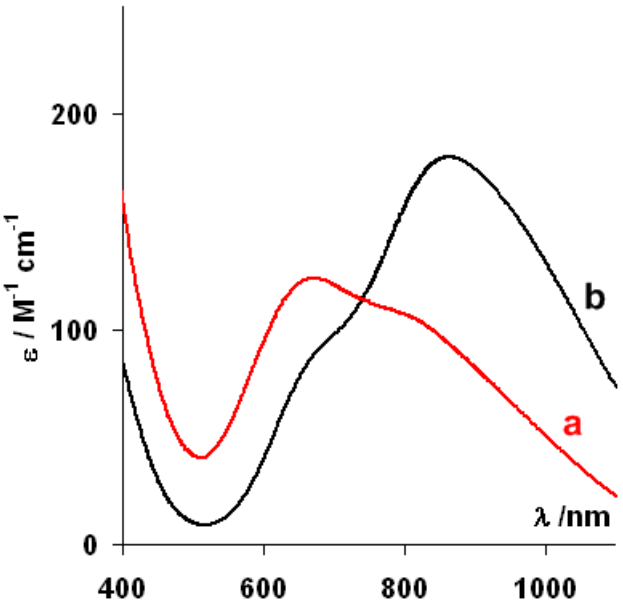

Fig. S6 UV-Vis spectra of a) $[Cu(6\text{-}eTMPA)(H_2O)](CF_3SO_3)_2$ (**4**) and b) $[Cu(TMPA)(H_2O)](CF_3SO_3)_2$ in DMF.

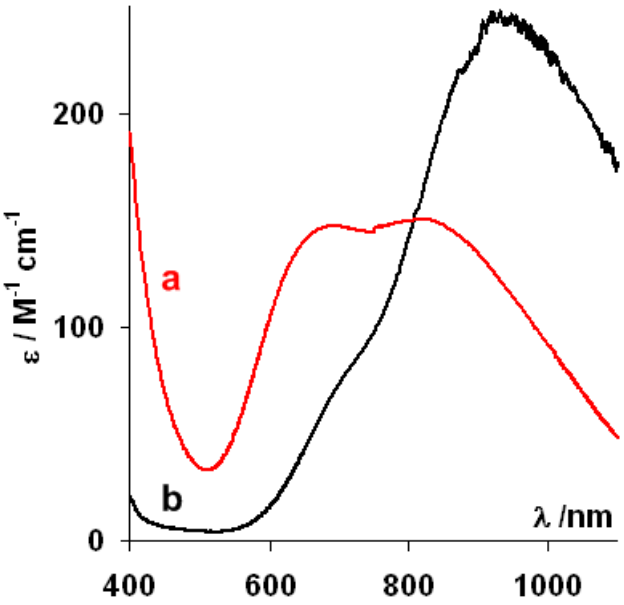

Fig. S7 UV-Vis spectra of a) $[Cu(6\text{-}eTMPA)(H_2O)](CF_3SO_3)_2$ (**4**) and b) $[Cu(TMPA)(H_2O)](CF_3SO_3)_2$ in CH_2Cl_2.

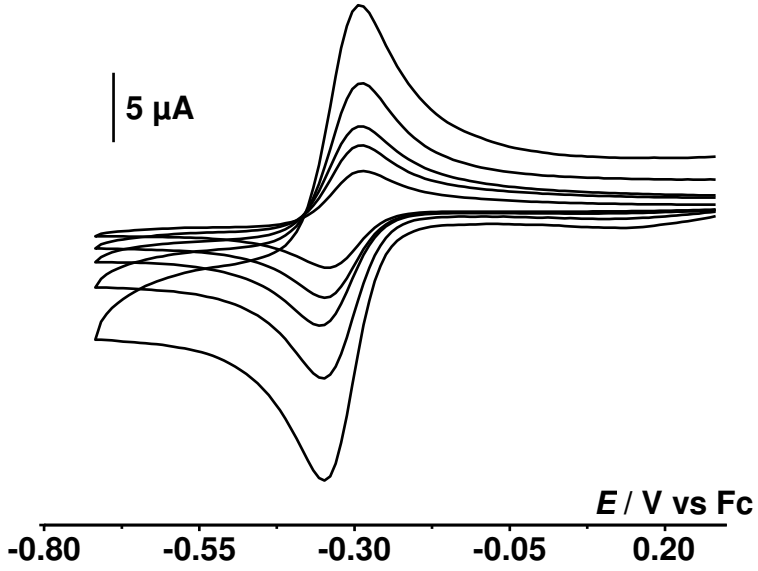

Fig. S8 Cyclic voltammograms at a Pt electrode (E /V vs Fc) of **4** in CH_3CN/NBu_4PF_6 ($0.02 < v < 0.5$ V s^{-1}). (C = 2 mM)

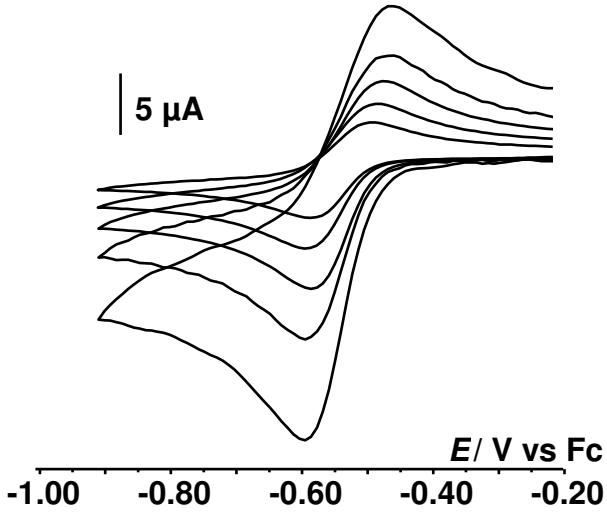

Fig. S9 Cyclic voltammogram at a Pt electrode (E /V vs Fc) of **4** in DMF/NBu_4PF_6 (0.02 < v < 0.5 V s^{-1}). (C = 2 mM)

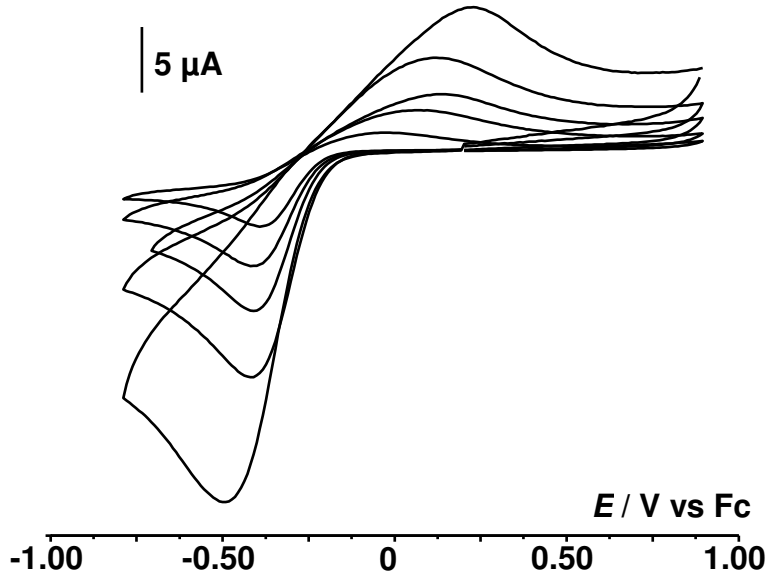

Fig. S10 Cyclic voltammograms at a Pt electrode (E /V vs Fc) of **4** in CH_2Cl_2/NBu_4PF_6 (0.02 < v < 0.5 V s^{-1}). (C = 2 mM).

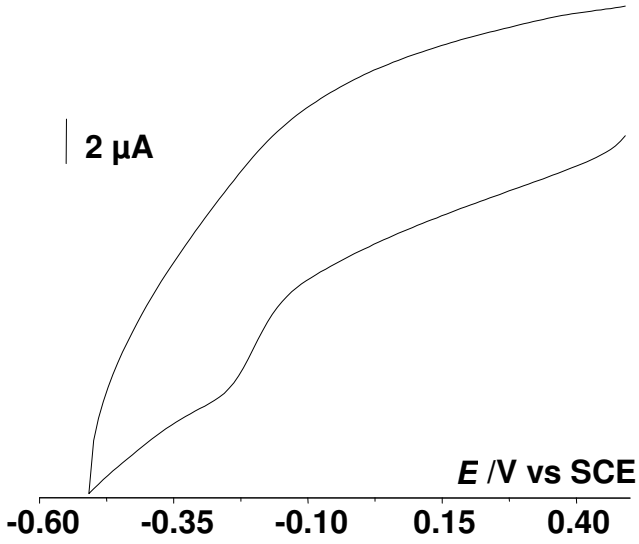

Fig. S11 Cyclic voltammograms at a vitreous carbon electrode (*E* /V vs SCE) of **4** in H_2O/KNO_3 (v = 0.1 V s^{-1}). (C = 1 mM).

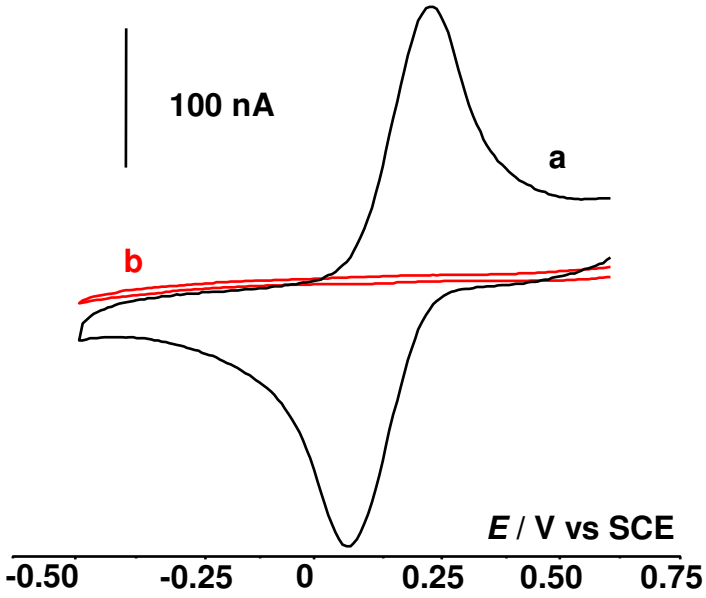

Fig. S12 Cyclic voltammogram at a a) bare Au electrode and b) azide-undecanethiol Au electrode in $H_2O/KNO_3 + K_3Fe(CN)_6$ (v = 0.1 V s^{-1}).

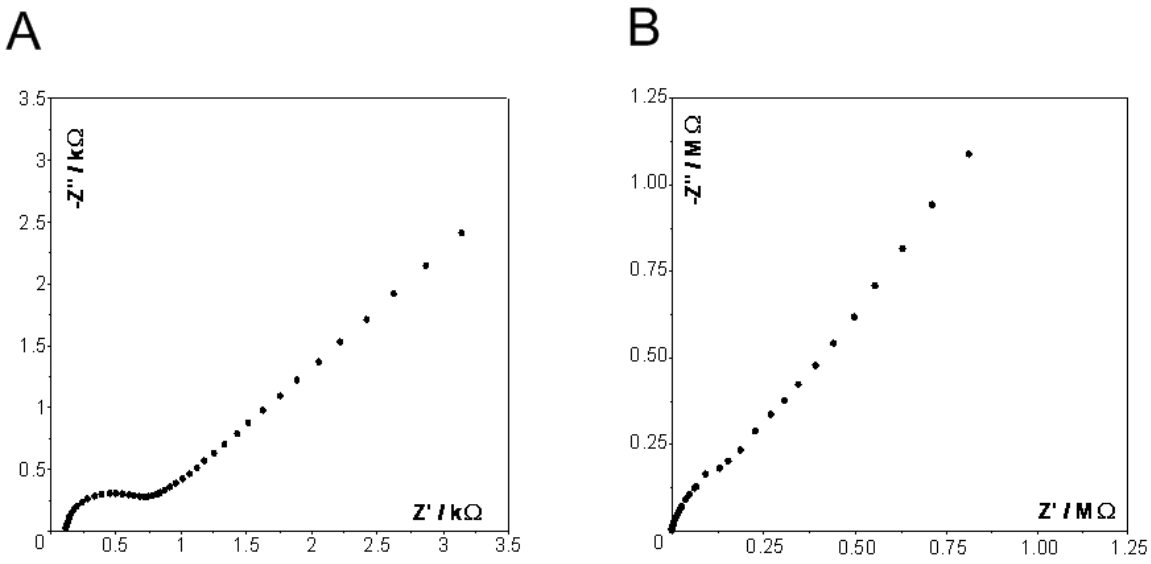

Fig. S13 AC Impedance complex-plane plots of a A) bare Au electrode and B) azide-undecanethiol Au electrode in H_2O/KNO_3 + $[Fe(CN)_6]K_3$ (C = 1 mM). AC amplitude E_{ac} 0.01 V. E_{dc} = 0.19 V vs SCE. 100 mHz < ω < 10 kHz. Electrode surface area: A = 0.07 cm^2.

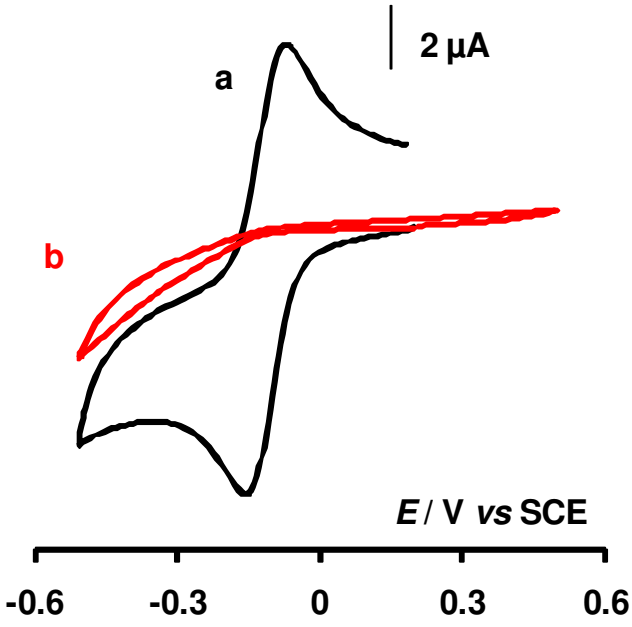

Fig. S14 Cyclic voltammogram at a a) bare Au electrode and b) azide-undecanethiol Au electrode in H_2O/KNO_3 + $[Ru(NH3)_6]Cl_3$ (ν = 0.1 V s^{-1}).

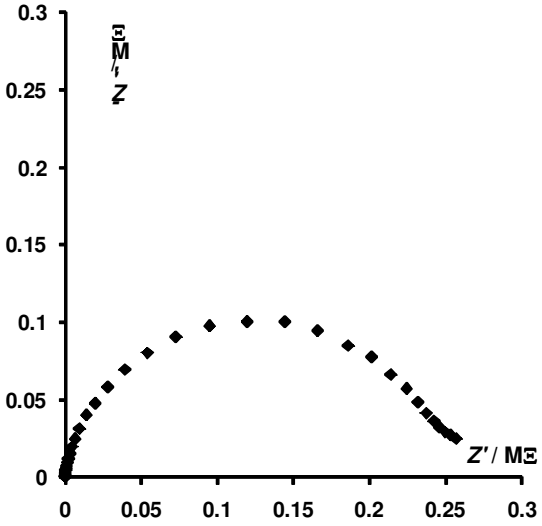

Fig. S15 AC Impedance complex-plane plots of an azide-undecanethiol Au electrode in H_2O/KNO_3 + $[Ru(NH_3)_6]Cl_3$. AC amplitude E_{ac} 0.01V. E_{dc} = -0.12 V vs SCE. 100 mHz < ω < 10 kHz. Electrode surface area: A = 0.07 cm^2.